IEEE Access
Multidisciplinary ⋮ Rapid Review ⋮ Open Access Journal

Received February 1, 2019, accepted February 14, 2019, date of publication February 21, 2019, date of current version March 7, 2019.

Digital Object Identifier 10.1109/ACCESS.2019.2900259

Correlation Receiver With Nonlinearity Blanking for DCSK Systems Under Pulse Jamming Attack

DUC-PHUC VUONG[1], DANG-KHANH LE[2], KHAC-KHIEM NGUYEN[1], AND BINH VAN NGUYEN[3,4]

[1]Department of Electric and Electronics Engineering, Vietnam Maritime University, Haiphong 180000, Vietnam
[2]VMU College, Vietnam Maritime University, Haiphong 180000, Vietnam
[3]Institute of Research and Development, Duy Tan University, Da Nang 550000, Vietnam
[4]School of Electrical Engineering and Computer Science, Gwangju Institute of Science and Technology, Gwangju 61005, South Korea

Corresponding author: Binh Van Nguyen (binhnguyen@gist.ac.kr)

ABSTRACT In this paper, we consider the fundamental and most studied non-coherent differential chaotic shift keying system under a pulse jamming environment. We devote our effort to propose a novel correlation receiver with nonlinearity blanking for the considered system to improve its anti-jamming performance. In addition and importantly, we also propose a mathematical framework to derive an optimal blanking threshold for the proposed receiver. The proposed nonlinearity blanking mechanism basically blocks the received signals with a larger amplitude than the blanking threshold, while the signals with a smaller amplitude are not affected at all. We then show that the proposed receiver with optimal blanking threshold significantly outperforms the conventional correlation counterpart.

INDEX TERMS Differential chaos shift keying, pulse jamming, correlation receiver, nonlinearity blanking, bit-error-rate.

I. INTRODUCTION

In traditional direct sequence - spread spectrum (DS-SS) systems, binary pseudo-noise (PN) sequences, i.e. m-sequences and Gold sequences, are extensively utilized as spreading sequences [1]. Although the PN sequences have a desirable auto-correlation property, their cross-correlation is poor due to large spikes occurring in the cross-correlation function. As a consequence, DS-SS systems suffer a self-jamming problem. More specifically, there are non-zero contributions from other users to another one in the same system. Another drawback of the PN sequences is their low level of security, i.e. they can be reconstructed by a linear regression attack [2]. To alleviate these drawbacks of DS-SS systems, chaotic communications (CC) is proposed. In CC systems, chaotic sequences are used to spread original data sequences. In addition, chaotic sequences are generated by chaotic generators (chaotic maps), i.e. tent and logistic maps. CC systems can be categorized as coherent and non-coherent ones. The former systems provide good performance, however, they require strict chaotic synchronization at destinations which limits their applications in reality. On the other hand, the latter systems give worse performance than that of the former ones, however, their deployment complexity is low, and thus, the non-coherent CC systems have been large investigated and found several applications in reality [3].

Differential chaotic shift keying (DCSK) is the most studied non-coherent chaotic modulation scheme. In a CC system with the DCSK scheme, referred to as DCSK system, each bit duration is divided into two equal slots. In the first slot, a reference sequence containing β chaotic samples is transmitted. In the second slot, either the reference sequence or its inverted version is sent depending on the value of the information bit. The performance of the DCSK system under noisy and multipath fading channels are carried out in [4]–[6]. It is shown that enlarging the spreading factor beyond a certain value degrades the system performance. In addition, the performance of the DCSK system under single-tone and pulse jamming environments are investigated in [7] and [8]. Lau *et al.* [7] show that the system performance is significantly degraded when the tone jamming frequency is an integer multiple of the bit frequency. Moreover, Khieu *et al.* [8] point out that the system performance does not depend on the pulse jamming duty cycle ρ when $\rho \leq 0.5$. However, when $\rho > 0.5$, enlarging ρ degrades the system performance. Furthermore, the DCSK system also finds several

The associate editor coordinating the review of this manuscript and approving it for publication was Walid Al-Hussaibi.

applications other practical systems, i.e. DCSK-based orthogonal frequency division multiplexing [9], DCSK-based cooperative communications [10], [11], DCSK-based multiple input multiple output [12], and DCSK-based pulse position modulation [13].

As another research trend, Kaddoum *et al.* [14] and Herceg *et al.* [24] propose several variants of the DCSK system. More specifically, Kaddoum *et al.* [14] introduce an improved DCSK (I-DCSK) system [14] to improve the data rate and the spectral efficiency of the DCSK system. In addition, Kaddoum *et al.* [15] present a short reference DCSK (SR-DCSK) system to improve the data rate and the energy efficiency of the DCSK system. Moreover, a noise reduction DCSK (NR-DCSK) system is proposed in [16]. Recently, the performance of the NR-DCSK system under broadband, partial-band, tone, and sweep jamming are analyzed in [17], in which the authors show that the single-tone jamming causes a more significant performance degradation than the multi-tone counterpart. In addition, the system performance is significantly degraded when the starting frequency of the sweep jammer is close to the carrier frequency of the transmitted chaotic signals, the sweep bandwidth is small, and the sweep time is half of the transmitted bit duration. In [18]–[20], multiresolution and multi-level DCSK systems are proposed. The multiresolution and multi-level DCSK systems can achieve a higher data rate, lower energy loss in reference sequence transmission, increased bandwidth, better security, and better bit error rate than the DCSK system. Furthermore, different combinations of index modulation and DCSK system are presented in [21]–[24]. The index modulation based DCSK systems significantly outperforms the DCSK one.

We observe that all aforementioned works only focuss on (i) analyzing the performance of existing CC systems, (ii) finding novel applications of the DCSK system in other practical systems, and (iii) proposing novel CC systems to alleviate drawbacks of existing ones. However, an important issue of mitigating effects of jamming signals on the performance of CC systems has only been recently discussed in [25]. When the jamming power is much bigger than that of legitimate chaotic signals, the inherent anti-jamming capability of CC systems may not work effectively, and thus, designing augmented jamming mitigation techniques for CC systems is of interest and paramount importance. Motivated by aforementioned facts, we here consider the DCSK system under the pulse jamming environment and design a novel correlation receiver with nonlinear blanking (NB) for it. In addition and importantly, we also propose a mathematical framework for deriving the optimal threshold value for the proposed receiver. Finally, we show that the proposed receiver with the optimal blanking threshold value significantly enhances the system performance. We focus on the DCSK system because it is the fundamental and most studied non-coherent CC system. In addition, it is widely integrated into other practical systems. It is noteworthy that, the correlation receiver with variational mode decomposition - independent component analysis - wavelet packet decomposition (VMD-ICA-WPD) presented in [25] is not applicable for the considered system since the ICA mechanism only performs well if original sources, i.e. chaotic and jamming signals, are non-Gaussian [26]. In addition, a blanking circuity is already proposed for the DCSK system in power line communications [27]. However, how to obtain an optimal threshold for the blanking mechanism is not presented in [27].

The remainder of this paper is organized as follows. Section II introduces the system and jamming models. Conventional correlation receiver is presented in the section III. In section IV, the proposed correlation receiver with NB is illustrated. In addition, the mathematical framework for deriving the optimal blanking threshold is also presented. Thereafter, representative simulations are provided in section V to demonstrate the advantages of the proposed receiver. Finally, our conclusion is given in section VI.

II. SYSTEM MODEL

The considered system contains a source S, a destination D, and a pulse jammer J, as illustrated in Fig. 1. All nodes are equipped with a single antenna and operate in the half duplex mode. The transmitted signal of the l^{th} bit b_l of S can be written as

$$s_k = \begin{cases} x_k, & \text{for } k = 2\beta\,(l-1)+1, \cdots, (2l-1)\,\beta, \\ b_l x_{k-\beta}, & \text{for } k = (2l-1)\,\beta+1, \cdots, 2l\beta, \end{cases} \tag{1}$$

where x_k denotes chaotic samples generated by the Tent map, i.e. $x_{k+1} = 2\min(x_k, 1-x_k)$ [4], [28].

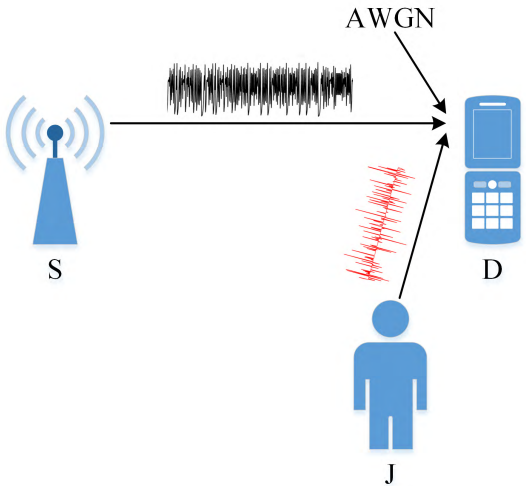

FIGURE 1. A DCSK system under an impulsive jamming attack.

The discrete baseband received signal at the destination D is given by

$$r_k = s_k + j_k + n_k, \tag{2}$$

where n_k is the zero-mean AWGN with variance $N_0/2$ and j_k denotes the pulse jamming signal. The jammer is assumed to

turn on and off periodically [8]. In addition, when the jammer is on, it emits Gaussian noise w_k with zero mean and power of P_j/ρ, where P_j is the average transmit power of the jammer and ρ is the jamming duty cycle. Mathematically, j_k can be written as

$$j_k = \begin{cases} w_k, & \text{for } k = 2(l-1)\beta+1, \cdots, 2(l-1)\beta+\lambda, \\ 0, & \text{for } k = 2(l-1)\beta+\lambda+1, \cdots, 2l\beta, \end{cases} \tag{3}$$

where $\lambda = \rho 2\beta$. We only consider the AWGN channel with jamming attack so that we can solely focus on jamming and design a NB receiver to mitigate its effects. The AWGN channel with jamming attack has been used in several recent related works on CC systems, i.e. [8] and [17].

III. CONVENTIONAL CORRELATION RECEIVER

A diagram illustration of the conventional correlation receiver of the DCSK system is given in the Fig. 2. More specifically, for each symbol, the received signal is correlated with its β sample - delay version. Then, the output B_l will be fed into a threshold detector. The transmitted bit will be decided to be 1 if $B_l \geq 0$, and 0 otherwise. The decision variable B_l can be written as

$$B_l = \sum_{k=2(l-1)\beta+1}^{(2l-1)\beta} r_k r_{k+\beta} = \underbrace{C_l}_{\text{desired signal}} + \underbrace{D_{1l} + D_{2l} + D_{3l}}_{\text{jamming}} + \underbrace{E_{1l} + E_{2l} + E_{3l} + E_{4l} + E_{5l}}_{\text{noise}}, \tag{4}$$

where

$$C_l = \sum_{k=2(l-1)\beta+1}^{(2l-1)\beta} b_l x_k^2, \tag{5}$$

$$\begin{bmatrix} D_{1l} \\ D_{2l} \\ D_{3l} \end{bmatrix} = \sum_{2(l-1)\beta+1}^{(2l-1)\beta} \begin{bmatrix} x_k j_{k+\beta} \\ b_l x_k j_k \\ j_k j_{k+\beta} \end{bmatrix}, \tag{6}$$

$$\begin{bmatrix} E_{1l} \\ E_{2l} \\ E_{3l} \\ E_{4l} \\ E_{5l} \end{bmatrix} = \sum_{2(l-1)\beta+1}^{(2l-1)\beta} \begin{bmatrix} x_k n_{k+\beta} \\ b_l x_k n_k \\ j_k n_{k+\beta} \\ n_k j_{k+\beta} \\ n_k n_{k+\beta} \end{bmatrix}. \tag{7}$$

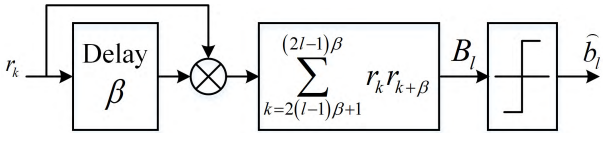

FIGURE 2. The conventional correlation receiver of the DCSK system.

IV. CORRELATION RECEIVER WITH NONLINEARITY BLANKING

In this section, we will present a novel correlation receiver with NB for the DCSK system under the pulse jamming environment. The proposed receiver is illustrated in the Fig. 3.

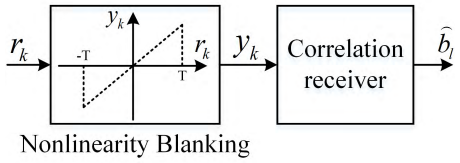

FIGURE 3. The proposed correlation receiver with nonlinearity blanking.

Particularly, the proposed receiver is a combination of a NB block and the conventional correlation receiver.

The operation of the NB block can be expressed as follows

$$y_k = \begin{cases} r_k, & \text{if } |r_k| \leq T, \\ 0, & \text{otherwise}, \end{cases} \tag{8}$$

where T is the NB threshold. The output of the NB block can be written as [29], [30]

$$y_k = \alpha s_k + d_k, \tag{9}$$

where α is a constant and d_k denotes the total distortion. α is chosen such that $E[d_k r_k] = 0$, and thus [30]

$$\alpha = E[y_k s_k] / E\left[(s_k)^2\right]. \tag{10}$$

In addition, the signal-to-interference-plus-noise-ratio (SINR) of the output of the NB block can be evaluated by using [30]

$$SINR_{NB} = \frac{E\left[(\alpha s_k)^2\right]}{E\left[(y_k - \alpha s_k)^2\right]} = \left[\frac{E\left[(y_k)^2\right]}{\alpha^2 E\left[(s_k)^2\right]} - 1\right]^{-1}. \tag{11}$$

It is natural that we should select T such that the above $SINR_{NB}$ is maximized. In order to do that, we need to derive analytical expressions of α and $SINR_{NB}$.

We now present a mathematical framework to derive an optimal threshold T. We first notice that x_k generated by the Tent map follows the uniform distribution on the interval [0, 1] [31]. In addition, we recall the definition of s_k given in (1). If $b_l = 1$, x_k appears twice during the bit b_l's duration. On the other hand, if $b_l = -1$, x_k appears once and $y_k = -x_k$ appears once during the bit b_l's duration. Since $b_l = 1$ and -1 with an equal probability of $1/2$, we can state that during the bit b_l's duration, x_k appears with a probability that is three times larger than that of y_k, which is uniformly distributed on $[-1, 0]$. As a result, the probability density distribution (PDF) of the transmitted signal can be expressed as

$$f_{s_k}(x) = \begin{cases} a_1 = 0.25, & \text{if } -1 \leq x \leq 0, \\ a_2 = 0.75, & \text{if } 0 < x \leq 1, \\ 0, & \text{otherwise}. \end{cases} \tag{12}$$

Consequently, we can also derive the conditional PDF of the received signal r_k as follows

$$f_{r_k}(x|I_i) = \frac{a_2 - a_1}{2} \text{erf}\left(\frac{x}{\sqrt{2\delta_{n_i}^2}}\right) + \frac{a_1}{2} \text{erf}\left(\frac{x+1}{\sqrt{2\delta_{n_i}^2}}\right) - \frac{a_2}{2} \text{erf}\left(\frac{x-1}{\sqrt{2\delta_{n_i}^2}}\right), \tag{13}$$

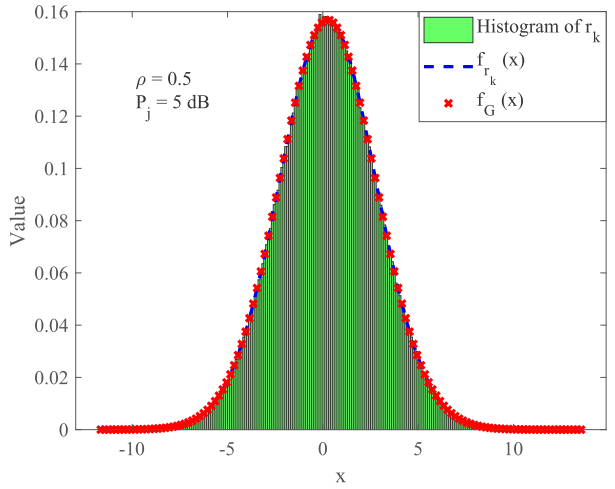

FIGURE 4. A comparison of PDF r_k and its approximation.

where $i = \{1, 2\}$, I_1 and I_2 respectively denote the condition that the jammer is on and off, $\delta_{n_2}^2 = N0/2$, $\delta_{n_1}^2 = N0/2 + P_j/\rho$, and erf $(\cdot)$ is the error function [32]. The proof is given in the Appendix A. Since the PDF of r_k is in a complex expression, it is challenging to proceed further. To find a simpler approximation of $f_{r_k}(x|I_i)$, we apply the series representation of the error function [32] and the binomial expansion into (13) and observe that $f_{r_k}(x|I_i)$ has a similar series representation to the Gaussian PDF, meaning that $f_{r_k}(x|I_i)$ can be well approximated by the Gaussian PDF. That is,

$$f_{r_k}(x|I_i) \simeq f_G(x|I_i) = \frac{1}{\sqrt{2\pi\delta_{G_i}^2}} \exp\left(-\frac{(x-\mu_G)^2}{2\delta_{G_i}^2}\right), \quad (14)$$

where $\mu_G = (a_2 - a_1)/2$ and $\delta_{G_i}^2 = 1/3 + \delta_{n_i}^2 - \mu_G^2$ are the mean and the variance of r_k, respectively. We derived μ_G and $\delta_{G_i}^2$ based on the original PDF given in (13). A double check of our approximation is given in the Fig. 4. It is clearly shown that the PDF of r_k is well approximated by the Gaussian PDF.

Secondly, we re-write $E[y_k s_k]$ as follows [30]

$$E[y_k s_k] = E[y_k s_k|C_1, I_1]\Pr[C_1, I_1] + E[y_k s_k|C_1, I_2]\Pr[C_1, I_2], \quad (15)$$

where C_1 denotes the event $|r_k| \le T$ and C_2 is the complement event of C_1. In addition, we have

$$E[y_k s_k|C_1, I_2] = \frac{1}{2}E\left[s_k^2|C_1, I_2\right] + \frac{1}{2}E\left[r_k^2|C_1, I_2\right] - \frac{1}{2}E\left[n_k^2|C_1, I_2\right], \quad (16)$$

where $E\left[s_k^2|C_1, I_2\right]$, $E\left[r_k^2|C_1, I_2\right]$, and $E\left[n_k^2|C_1, I_2\right]$ are given in (17)-(19), as shown at the bottom of this page, where $A_1 = \text{erf}\left(\frac{T+\mu_G}{\sqrt{2\delta_{G_2}^2}}\right)$, $A_2 = \text{erf}\left(\frac{T-\mu_G}{\sqrt{2\delta_{G_2}^2}}\right)$, $A_3 = \text{erf}\left(\frac{T-1}{\sqrt{2\delta_{n_2}^2}}\right)$, and $A_4 = \text{erf}\left(\frac{T+1}{\sqrt{2\delta_{n_2}^2}}\right)$. The detailed derivations of (16)-(19) are provided in the appendix B-E, respectively. Moreover, the probability $\Pr[C_1, I_2]$ is obtained as

$$\begin{aligned}\Pr[C_1, I_2] &= \Pr[-T \le r_k \le T|I_2]\Pr[I_2] \\ &= \frac{(1-\rho)}{\sqrt{2\pi\delta_{G_2}^2}} \int_{-T}^{T} \exp\left(-\frac{(x-\mu_G)}{2\delta_{G_2}^2}\right) dx \\ &= \frac{1-\rho}{2}(A_1 + A_2). \end{aligned} \quad (20)$$

Plugging (17)-(19) into (16) and multiplying the outcome by (20) we obtain the second term in the right hand-side (RHS) of (15), given in (21) as hown at the top of the next page. We now turn our interest to the first term given in the RHS of (15). Similar to (16), we have

$$E[y_k s_k|C_1, I_1] = \frac{1}{2}E\left[s_k^2|C_1, I_1\right] + \frac{1}{2}E\left[r_k^2|C_1, I_1\right] - \frac{1}{2}E\left[n_k^2|C_1, I_1\right]. \quad (22)$$

It is noteworthy that we can readily obtain expressions of $E\left[s_k^2|C_1, I_1\right]$, $E\left[r_k^2|C_1, I_1\right]$, and $E\left[n_k^2|C_1, I_1\right]$ by replacing $\delta_{n_2}^2$ and δ_{G_2} in (17)-(19) with $\delta_{n_1}^2$ and $\delta_{G_1}^2$. In addition, $\Pr[C_1, I_1]$ can also be obtained from (20) by replacing $(1-\rho)$ with ρ, and $\delta_{n_2}^2$ and $\delta_{G_2}^2$ with $\delta_{n_1}^2$ and $\delta_{G_1}^2$. As a result, we can obtain an expression of $E[y_k s_k|C_1, I_1]\Pr[C_1, I_1]$ as in (23), as shown in the top of the next page, where $A_1' = \text{erf}\left(\frac{T+\mu_G}{\sqrt{2\delta_{G_1}^2}}\right)$, $A_2' = \text{erf}\left(\frac{T-\mu_G}{\sqrt{2\delta_{G_1}^2}}\right)$, $A_3' = \text{erf}\left(\frac{T-1}{\sqrt{2\delta_{n_1}^2}}\right)$, and $A_4' = \text{erf}\left(\frac{T+1}{\sqrt{2\delta_{n_1}^2}}\right)$.

$$E\left[s_k^2|C_1, I_2\right] = \frac{1}{A_1 + A_2}\left[\frac{1-T^3-3T\delta_{n_2}^2}{3}A_3 + \frac{1+T^3+3T\delta_{n_2}^2}{3}A_4 - \sqrt{\frac{8\delta_{n_2}^2}{9\pi}}e^{-\frac{T^2+1}{2\delta_{n_2}^2}} \cdot \left(T\cosh\left(\frac{T}{\delta_{n_2}^2}\right) + \left(1 + T^2 + 2\delta_{n_2}^2\right)\sinh\left(\frac{T}{\delta_{n_2}^2}\right)\right)\right], \quad (17)$$

$$E\left[r_k^2|C_1, I_2\right] = \frac{\sqrt{2}}{\sqrt{\pi\delta_{G_2}^2}(A_1 + A_2)}\left[\delta_{G_2}^2 e^{-\frac{(T+\mu_G)^2}{2\delta_{G_2}^2}}\left(\mu_G - T - (T + \mu_G)e^{\frac{2T\mu_G}{\delta_{G_2}^2}}\right) + \sqrt{\frac{\pi\delta_{G_2}^2}{2}}\left(\mu_G^2 + \delta_{G_2}^2\right)(A_1 + A_2)\right], \quad (18)$$

$$E\left[n_k^2|C_1, I_2\right] = \frac{\delta_{n_2}^2}{\sqrt{2\pi}(A_1 + A_2)}\left[4\delta_{n_2}e^{-\frac{(T+1)^2}{2\delta_{n_2}^2}}\left(1 - e^{\frac{2T}{\delta_{n_2}^2}}\right) + \sqrt{2\pi}\left((1-T)A_3 + (T+1)A_4\right)\right]. \quad (19)$$

$$E\left[y_k s_k|C_1,I_2\right]\Pr\left[C_1,I_2\right]=\left[\frac{1}{2}\left[\begin{array}{l}\frac{1-T^3-3T\delta_{n_2}^2}{3}A_3+\frac{1+T^3+3T\delta_{n_2}^2}{3}A_4-\sqrt{\frac{8\delta_{n_2}^2}{9\pi}}e^{-\frac{T^2+1}{2\delta_{n_2}^2}}\\ \cdot\left(T\cosh\left(\frac{T}{\delta_{n_2}^2}\right)+\left(1+T^2+2\delta_{n_2}^2\right)\sinh\left(\frac{T}{\delta_{n_2}^2}\right)\right)\end{array}\right]\right.$$
$$+\frac{1}{\sqrt{2\pi\delta_{G_2}^2}}\left[\delta_{G_2}^2 e^{-\frac{(T+\mu_G)^2}{2\delta_{G_2}^2}}\left(\mu_G-T+(T+\mu_G)\,e^{\frac{2T\mu_G}{\delta_{G_2}^2}}\right)+\sqrt{\frac{\pi\delta_{G_2}^2}{2}}\left(\mu_G^2+\delta_{G_2}^2\right)(A_1+A_2)\right]$$
$$\left.-\frac{\delta_{n_2}^2}{2\sqrt{2\pi}}\left[4\delta_{n_2}e^{-\frac{(T+1)^2}{2\delta_{n_2}^2}}\left(1-e^{\frac{2T}{\delta_{n_2}^2}}\right)+\sqrt{2\pi}\left((1-T)A_3+(T+1)A_4\right)\right]\right]\frac{1-\rho}{2}. \quad (21)$$

$$E\left[y_k s_k|C_1,I_1\right]\Pr\left[C_1,I_1\right]=\left[\frac{1}{2}\left[\begin{array}{l}\frac{1-T^3-3T\delta_{n_1}^2}{3}A'_3+\frac{1+T^3+3T\delta_{n_1}^2}{3}A'_4-\sqrt{\frac{8\delta_{n_1}^2}{9\pi}}e^{-\frac{T^2+1}{2\delta_{n_1}^2}}\\ \cdot\left(T\cosh\left(\frac{T}{\delta_{n_1}^2}\right)+\left(1+T^2+2\delta_{n_1}^2\right)\sinh\left(\frac{T}{\delta_{n_1}^2}\right)\right)\end{array}\right]\right.$$
$$+\frac{1}{\sqrt{2\pi\delta_{G_1}^2}}\left[\delta_{G_1}^2 e^{-\frac{(T+\mu_G)^2}{2\delta_{G_1}^2}}\left(\mu_G-T+(T+\mu_G)\,e^{\frac{2T\mu_G}{\delta_{G_1}^2}}\right)+\sqrt{\frac{\pi\delta_{G_1}^2}{2}}\left(\mu_G^2+\delta_{G_1}^2\right)\left(A'_1+A'_2\right)\right]$$
$$\left.-\frac{\delta_{n_1}^2}{2\sqrt{2\pi}}\left[4\delta_{n_1}e^{-\frac{(T+1)^2}{2\delta_{n_1}^2}}\left(1-e^{\frac{2T}{\delta_{n_1}^2}}\right)+\sqrt{2\pi}\left((1-T)A'_3+(T+1)A'_4\right)\right]\right]\frac{\rho}{2}. \quad (23)$$

Finally, an expression of α is obtained by plugging (21) and (23) into (15) and then plugging the outcome into (10), noting that $E\left[s_k^2\right]=1/3$.

On the other hand, to derive an expression of $SINR_{NB}$, we re-write $E\left[y_k^2\right]$ as follows

$$E\left[y_k^2\right]=E\left[y_k^2|C_1,I_1\right]\Pr\left[C_1,I_1\right]+E\left[y_k^2|C_1,I_2\right]\Pr\left[C_1,I_2\right]. \quad (24)$$

Since given the event C_1, $y_k = r_k$, (24) can be readily derived by using (18) and (20). It means that $SINR_{NB}$ can also be obtained by using the afore-presented results. Then, the optimal blanking threshold can be found as follows

$$T_{opt}=\arg\min_{T}\left(\frac{E\left[y_k^2\right]}{\alpha^2}\right). \quad (25)$$

Since $E\left[y_k^2\right]$ and α are in complex expressions, it is challenging to obtain a closed form solution for the above minimization problem. However, the above problem can be readily solved by using a numerical method, i.e. the quasi-Newton method with the Broydon-Fletcher-Goldfarb-Shanno update formula or the brute-force search method. Noting that numerical solution of (25) does not pose any computational difficulties. With this in mind, the proposed receiver accompanied by an online numerical method can be readily deployed in practical applications. In case of fading channels, the proposed receiver may also be applicable with a channel estimation and equalization mechanism is done in advanced. However, the performance improvement is expected to be much less than that obtained in the AWGN channel, since the blanking threshold is optimized under the AWGN condition. The issue of optimal blanking threshold under multi-path fading channels will be investigated in our future works.

V. SIMULATION RESULTS

In this section, representative simulation results will be provided to illustrate the advantages of the proposed anti-jamming correlation receiver with NB for the DCSK system under the pulse jamming environment. The simulation setting follows the system model presented in the section II with $\beta = 200$ and jamming-to-signal-power-ratio (JSR) = 15 dB, unless explicitly mentioned otherwise.

In Fig. 5, we present α as a function of the blanking threshold T with several values of ρ. In the simulation, we set Eb/N0 = 15 dB. It is firstly shown that our analysis results follow the simulated ones excellently. In addition, it is illustrated that α approaches one when the threshold T increases, as expected. The reason is that as T goes large, the NB block does nothing. In other words, in this case, the NB block's input is equal to the NB block's output, and thus, $\alpha = 1$.

We now present the output SINR of the NB block, $SINR_{NB}$ versus the blanking threshold T with several values of the jamming duty cycle in Fig. 6. In the simulation, we set Eb/N0 = 15 dB. It is first illustrated that for each value of ρ, there exists an optimum blanking threshold that maximizes the $SINR_{NB}$. Noting that the maximum $SINR_{NB}$ is obtained when the useful signal is kept as much as possible. Secondly, the figure also shows that as ρ increases, the output SINR of the NB block reduces. The reason is that, as ρ increases, more

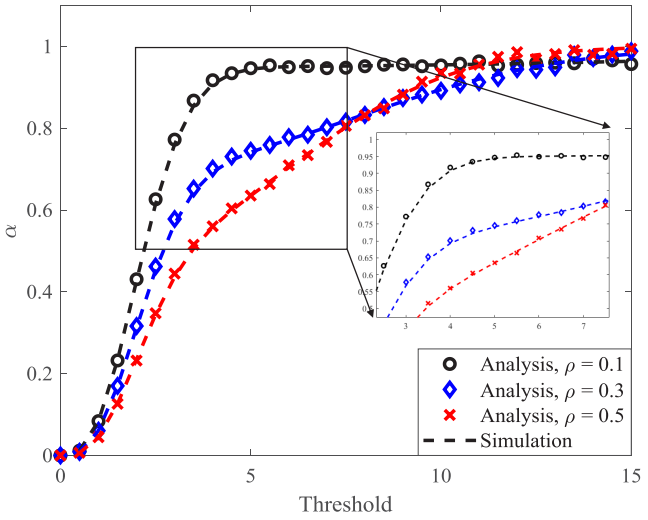

FIGURE 5. α versus the blanking threshold T.

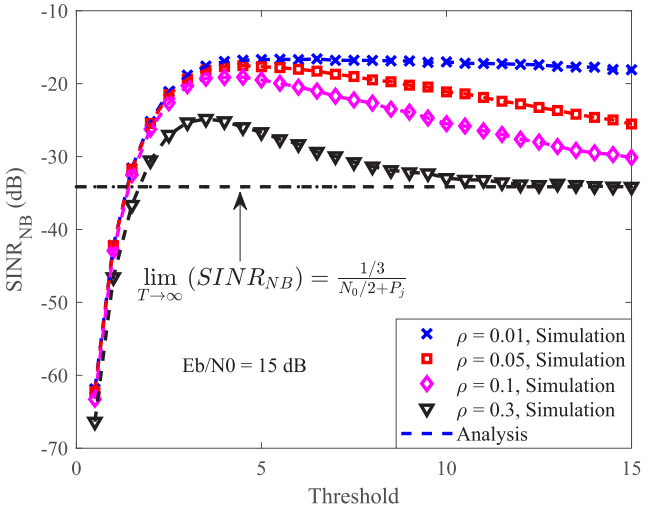

FIGURE 6. $SINR_{NB}$ versus the blanking threshold T.

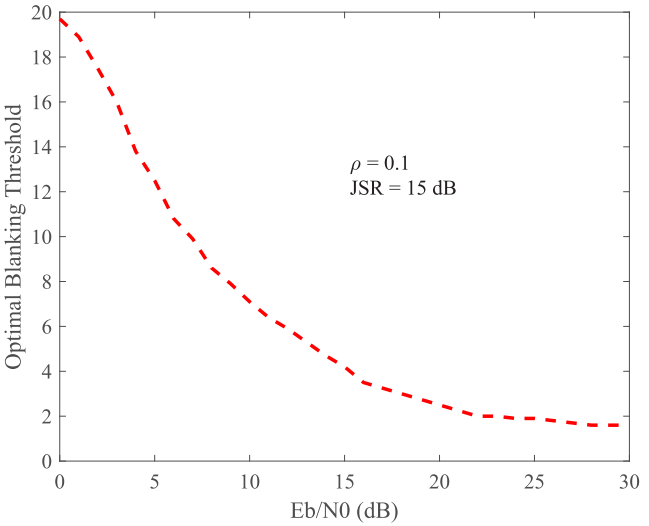

FIGURE 7. Optimal blanking threshold versus $Eb/N0$.

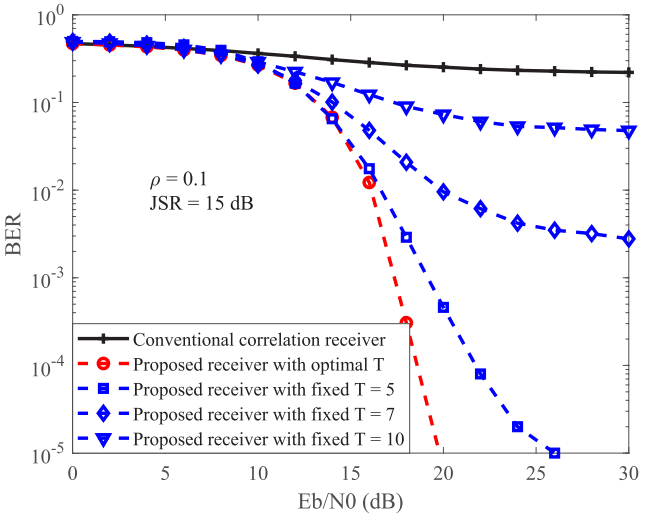

FIGURE 8. BER performance of the DCSK system versus $Eb/N0$.

and more transmitted chaotic samples are jammed, and thus, the SINR of the received signal as well as the SINR of the output of the NB block reduces. Thirdly, it is noted that as T goes to infinity, the output SINR of the NB block converges to a saturated value being equal to $\frac{1/3}{N_0/2+P_j}$, and the larger ρ the faster the saturation.

The optimal blanking threshold versus Eb/N0 with $\rho = 0.1$ is illustrated in Fig. 7. We observe that as Eb/N0 increases, the optimal blanking threshold decreases and converges to a certain value. A possible explanation is as follows. As Eb/N0 enlarges, the power of AWGN noise is reduced. As a result, the amplitude of the summation of the transmitted chaotic signal and AWGN noise is reduced, which makes the optimal blanking threshold reduces and converges to a certain value.

The BER performance of the DCSK system provided by the conventional correlation receiver and the proposed correlation receiver with NB versus Eb/N0 is presented in Fig. 8. In the simulation, we set $\rho = 0.1$. It is first shown that the conventional correlation receiver provides the worst BER which converges around 0.3 even with high Eb/N0 values. Noting that this level of BER is not preferred at all in CC-based applications, i.e. ultra wide band wireless communications. On the other hand, the proposed correlation receivers with NB significantly enhance the system performance, especially the one with optimal blanking threshold. It is also noteworthy that the operation of the NB block is quite simple, meaning that the computation complexity of the proposed receiver is comparable with that of the conventional correlation receiver. In a summary, a significant BER enhancement and a comparable computation complexity suggest that the proposed receiver is highly applicable for practical CC systems. It is also noteworthy that without jamming, the proposed receiver provides a similar performance

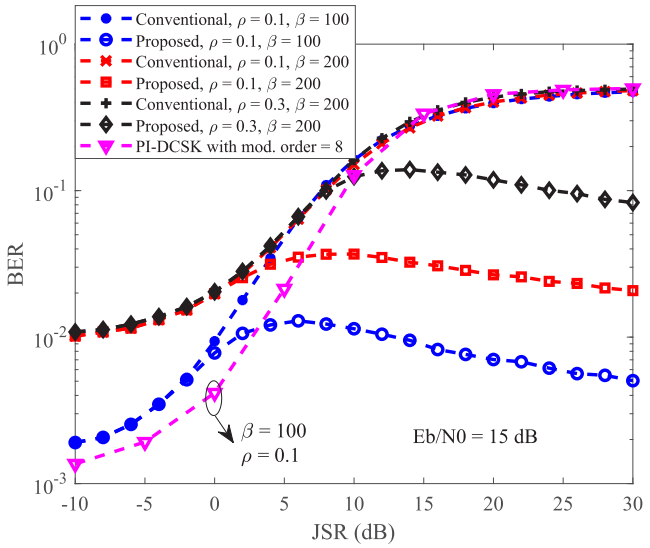

FIGURE 9. BER performance of the DCSK system versus JSR.

to that of the conventional one, which is not shown here for brevity.

We now illustrate the effects of ρ, β, and JSR on the performance of the proposed receiver in Fig. 9. For a benchmark comparison, the performance of the PI-DCSK [23] system with 8-modulation order, is also plotted. It is firstly shown that increasing β degrades the system performances provided by both the conventional and the proposed receivers. The possible reason is that as β increases, it is possibly that more transmitted samples are corrupted by noise and jamming. Secondly, it is observed that increasing JSR degrades the system performance provided by the conventional correlation receiver. On the other hand, as JSR increases, the system performance provided by the proposed receiver is first degraded but then improved. The reason is that as JSR is large enough, amplitudes of transmitted samples corrupted by noise and jamming are more likely to exceed the blanking threshold, then those samples are readily detected and set to zero, and thus, the system performance is enhanced. Thirdly, we also notice that with small value of ρ (i.e. $\rho = 0.1$), the proposed receiver outperforms the conventional one even when JSR = 0 dB. However, as ρ enlarges, a higher value of JSR is required so that the proposed receiver can show its advantages. This means that the proposed receiver works well in scenarios where the pulse jamming is not dense in time. In cases of dense pulse jamming signals, i.e. with $\rho \geq 0.7$, the proposed receiver may suppress a large portions of useful signals, and thus, cannot provide any advantages compared to the conventional counterpart. Finally, it is pointed out that the DCSK system with the proposed receiver also significantly outperforms the recent advanced PI-DCSK system in the medium and high JSR regions.

VI. CONCLUSION

In this work, we considered the fundamental and most studied non-coherent DCSK system under the pulse jamming environment. To improve the system performance, we designed a novel correlation receiver with nonlinearity blanking. In addition and importantly, we proposed a mathematical framework to obtain the optimal blanking threshold for the proposed receiver. We showed that the proposed receiver significantly outperforms the conventional correlation one. More specifically, with $\beta = 200$, $\rho = 0.1$, JSR = 15 dB, and Eb/N0 = 20 dB the proposed receiver with optimal blanking threshold provides a BER being equal to 10^{-5}, while the conventional correlation counterpart gives a BER being equal to 0.3.

APPENDIX A
A DERIVATION OF (13)

Let's first define $w_k = n_k + j_k$, whose conditional PDF is given by

$$f_{w_k}(x|I_i) = \frac{1}{\sqrt{2\pi\delta_{n_i}^2}} \exp\left(\frac{-x^2}{2\delta_{n_i}^2}\right), \tag{26}$$

where $i = \{1, 2\}$, I_1 and I_2 denote the conditions that jammer is one and off, $\delta_{n_1}^2 = N_0/2 + P_j/\rho$, and $\delta_{n_2}^2 = N_0/2$. Then, we derive the conditional PDF of r_k as follows

$$\begin{aligned} f_{r_k}(x|I_i) &= \int_{-\infty}^{\infty} f_{s_k}(x-y) f_{w_k}(y|I_i)\, dy \\ &= \frac{a_1}{\sqrt{2\pi\delta_{n_i}^2}} \int_{-1}^{0} \exp\left(-\frac{(x-y)^2}{2\delta_{n_i}^2}\right) dy \\ &\quad + \frac{a_2}{\sqrt{2\pi\delta_{n_i}^2}} \int_{0}^{1} \exp\left(-\frac{(x-y)^2}{2\delta_{n_i}^2}\right) dy \\ &= \frac{a_2 - a_1}{2} erf\left(\frac{x}{\sqrt{2\delta_{n_i}^2}}\right) + \frac{a_1}{2} erf\left(\frac{x+1}{\sqrt{2\delta_{n_i}^2}}\right) \\ &\quad - \frac{a_2}{2} erf\left(\frac{x-1}{\sqrt{2\delta_{n_i}^2}}\right). \end{aligned} \tag{27}$$

APPENDIX B
A DERIVATION OF (16)

Given the event C_1, we have $y_k = s_k + n_k$, and thus

$$E[y_k s_k | C_1, I_2] = E\left[s_k^2 | C_1, I_2\right] + E[s_k n_k | C_1, I_2]. \tag{28}$$

In addition, since $r_k = s_k + n_k$, we have $r_k^2 = s_k^2 + 2 s_k n_k + n_k^2$, and thus

$$s_k n_k = \frac{1}{2}\left(r_k^2 - s_k^2 - n_k^2\right). \tag{29}$$

Consequently,

$$\begin{aligned} E[s_k n_k | C_1, I_2] &= \frac{1}{2} E\left[r_k^2 | C_1, I_2\right] - \frac{1}{2} E\left[s_k^2 | C_1, I_2\right] \\ &\quad - \frac{1}{2} E\left[n_k^2 | C_1, I_2\right]. \end{aligned} \tag{30}$$

Finally, combining (28) and (30) gives (16).

APPENDIX C
A DERIVATION OF (17)

First, we extend $E\left[s_k^2|C_1, I_2\right]$ as follows

$$E\left[s_k^2|C_1, I_2\right] = \int_{-1}^{0} s_k^2 f_{s_k}\left(x|C_1, I_2\right) dx + \int_{0}^{1} s_k^2 f_{s_k}\left(x|C_1, I_2\right) dx, \quad (31)$$

where

$$f_{s_k}\left(x|C_1, I_2\right) = \frac{f_{s_k}\left(x\right) \Pr\left[-T \le r_k \le T|s_k, I_2\right]}{\Pr\left[-T \le r_k \le T|I_2\right]}. \quad (32)$$

The probability term given in the numerator of (32), denoted as Prob_{nu}, is obtained as

$$\begin{aligned}\text{Prob}_{\text{nu}} &= \int_{-T}^{T} \frac{1}{\sqrt{2\pi\delta_{n_2}^2}} \exp\left(-\frac{(x-s_k)^2}{2\delta_{n_2}^2}\right) dx \\ &= \frac{1}{2}\left[erf\left(\frac{T-s_k}{\sqrt{2\pi\delta_{n_2}^2}}\right) + erf\left(\frac{T+s_k}{\sqrt{2\pi\delta_{n_2}^2}}\right)\right]. \quad (33)\end{aligned}$$

Similarly, the probability term given in the denominator of (32), denoted as Prob_{de}, is given by

$$\begin{aligned}\text{Prob}_{\text{de}} &= \int_{-T}^{T} \frac{1}{\sqrt{2\pi\delta_{G_2}^2}} \exp\left(-\frac{(x-\mu_G)^2}{2\delta_{G_2}^2}\right) dx \\ &= \frac{1}{2}\left[erf\left(\frac{T-\mu_G}{\sqrt{2\pi\delta_{G_2}^2}}\right) + erf\left(\frac{T+\mu_G}{\sqrt{2\pi\delta_{G_2}^2}}\right)\right]. \quad (34)\end{aligned}$$

Then, plugging (33), (34), and (12) into (32) and (31) with tedious manipulation yields (17).

APPENDIX D
A DERIVATION OF (18)

$E\left[r_k^2|C_1, I_2\right]$ can be further extended as follows

$$E\left[r_k^2|C_1, I_2\right] = \int_{-T}^{T} x^2 f_{r_k}\left(x|C_1, I_2\right) dx, \quad (35)$$

where

$$f_{r_k}\left(x|C_1, I_2\right) = f_{r_k}\left(x|I_2\right) / \Pr\left[C_1|I_2\right], \quad (36)$$

$$f_{r_k}\left(x|I_2\right) = \frac{1}{\sqrt{2\pi\delta_{G_2}^2}} \exp\left(-\frac{(x-\mu_G)^2}{2\delta_{G_2}^2}\right), \quad (37)$$

and $\Pr\left[C_1|I_2\right] = \text{Prob}_{\text{de}}$. Finally, combining all the results with some manipulation gives (18).

APPENDIX E
A DERIVATION OF (19)

$E\left[n_k^2|C_1, I_2\right]$ can be re-written as

$$E\left[n_k^2|C_1, I_2\right] = \int_{-\infty}^{\infty} x^2 f_{n_k}\left(x|C_1, I_2\right) dx, \quad (38)$$

where

$$f_{n_k}\left(x|C_1, I_2\right) = \frac{f_{n_k}\left(x|I_2\right) \Pr\left[C_1|n_k, I_2\right]}{\Pr\left[C_1|I_2\right]}, \quad (39)$$

$$f_{n_k}\left(x|I_2\right) = \frac{1}{\sqrt{2\pi\delta_{n_2}^2}} \exp\left(-\frac{x^2}{2\delta_{n_2}^2}\right), \quad (40)$$

and $\Pr\left[C_1|I_2\right] = \text{Prob}_{\text{de}}$. In addition, the probability term given in the numerator of (39) is extended as

$$\Pr\left[C_1|n_k, I_2\right] = \int_{-T}^{T} f_{s_k}\left(x|n_k, I_2\right) dx. \quad (41)$$

After considering all possible values of n_k, we obtain

$$\Pr\left[C_1|n_k, I_2\right] = \begin{cases} 0, & \text{if } n_k < -T-1 \text{ or } n_k > T+1 \\ 1, & \text{if } 1 < n_k < T-1 \\ a_2\left(T+1+n_k\right), & \text{if } -T-1 < n_k < -T \\ a_1\left(n_k+T\right)+a_2, & \text{if } -T < n_k < -T+1 \\ a_1+a_2\left(T-n_k\right), & \text{if } T-1 < n_k < T \\ a_1\left(T+1-n_k\right), & \text{if } T < n_k < T+1 \end{cases} \quad (42)$$

Finally, combining all the results with some manipulation gives (19).

REFERENCES

[1] S. Hara and R. Prasad, "Overview of multicarrier CDMA," *IEEE Commun. Mag.*, vol. 35, no. 12, pp. 126–133, Dec. 1997.
[2] G. Kaddoum, "Wireless chaos-based communications systems: A comprehensive survey," *IEEE Access*, vol. 4, pp. 2621–2648, May 2016.
[3] Y. Fang, G. Han, P. Chen, F. C. M. Lau, G. Chen, and L. Wang, "A survey on DCSK-based communication systems and their application to UWB scenarios," *IEEE Commun. Surveys Tut.*, vol. 18, no. 3, pp. 1804–1837, 3rd Quart., 2016.
[4] M. Sushchik, L. S. Tsimring, and A. R. Volkovskii, "Performance analysis of correlation-based communication schemes utilizing chaos," *IEEE Trans. Circuits Syst. I, Fundam. Theory Appl.*, vol. 47, no. 12, pp. 1684–1691, Dec. 2000.
[5] Y. Xia, C. K. Tse, and F. C. M. Lau, "Performance of differential chaos-shift-keying digital communication systems over a multipath fading channel with delay spread," *IEEE Trans. Circuits Syst. II, Exp. Briefs*, vol. 51, no. 12, pp. 680–684, Dec. 2004.
[6] M. Long, Y. Chen, and F. Peng, "Simple and accurate analysis of BER performance for DCSK chaotic communication," *IEEE Commun. Lett.*, vol. 15, no. 11, pp. 1175–1177, Nov. 2011.
[7] F. C. M. Lau, M. Ye, C. K. Tse, and S. F. Hau, "Anti-jamming performance of chaotic digital communication systems," *IEEE Trans. Circuits Syst. I, Fundam. Theory Appl.*, vol. 49, no. 10, pp. 1486–1494, Oct. 2002.
[8] H. T. Khieu, D.-K. Le, and B. Van Nguyen, "On the performance analysis of a DCSK system under the pulse jamming environment," *PLoS One*, vol. 13, no. 8, pp. 1–11, Aug. 2018.
[9] G. Kaddoum, "Design and performance analysis of a multiuser OFDM based differential chaos shift keying communication system," *IEEE Trans. Commun.*, vol. 64, no. 1, pp. 249–260, Jan. 2016.

[10] W. Xu, L. Wang, and G. Chen, "Performance of DCSK cooperative communication systems over multipath fading channels," *IEEE Trans. Circuits Syst. I, Reg. Papers*, vol. 58, no. 1, pp. 196–204, Jan. 2011.
[11] G. Cai, Y. Fang, G. Han, J. Xu, and G. Chen, "Design and analysis of relay-selection strategies for two-way relay network-coded DCSK systems," *IEEE Trans. Veh. Technol.*, vol. 67, no. 2, pp. 1258–1271, Feb. 2018.
[12] Y. Fang, L. Xu, L. Wang, and G. Chen, "Performance of MIMO relay DCSK-CD systems over Nakagami fading channels," *IEEE Trans. Circuits Syst. I, Reg. Papers*, vol. 60, no. 3, pp. 757–767, Mar. 2013.
[13] M. Miao, L. Wang, M. Katz, and W. Xu, "Hybrid modulation scheme combining PPM with differential chaos shift keying modulation," *IEEE Wireless Commun. Lett.*, to be published. doi: 10.1109/LWC.2018.2871137.
[14] G. Kaddoum, E. Soujeri, C. Arcila, and K. Eshteiwi, "I-DCSK: An improved noncoherent communication system architecture," *IEEE Trans. Circuits Syst. II, Exp. Briefs*, vol. 62, no. 9, pp. 901–905, Sep. 2015.
[15] G. Kaddoum, E. Soujeri, and Y. Nijsure, "Design of a short reference noncoherent chaos-based communication systems," *IEEE Trans. Commun.*, vol. 64, no. 2, pp. 680–689, Jan. 2016.
[16] G. Kaddoum and E. Soujeri, "NR-DCSK: A noise reduction differential chaos shift keying system," *IEEE Trans. Circuits Syst., II, Exp. Briefs*, vol. 63, no. 7, pp. 648–652, Jul. 2016.
[17] B. Van Nguyen, H. Jung, and K. Kim, "On the antijamming performance of the NR-DCSK system," *Secur. Commun. Netw.*, vol. 2018, pp. 1–8, Feb. 2018.
[18] L. Wang, G. Cai, and G. R. Chen, "Design and performance analysis of a new multiresolution M-ary differential chaos shift keying communication system," *IEEE Trans. Wireless Commun.*, vol. 14, no. 9, pp. 5197–5208, Sep. 2015.
[19] H. Yang, W. K. S. Tang, G. Chen, and G.-P. Jiang, "System design and performance analysis of orthogonal multi-level differential chaos shift keying modulation scheme," *IEEE Trans. Circuits Syst. I, Reg. Papers*, vol. 63, no. 1, pp. 146–156, Jan. 2016.
[20] G. Cai, Y. Fang, G. Han, L. Wang, and G. Chen, "A new hierarchical M-ary DCSK communication system: design and analysis," *IEEE Trans. Circuits Syst., I, Reg. Papers*, vol. 58, no. 1, pp. 196–206, Jan. 2011.
[21] W. Xu, T. Huang, and L. Wang, "Code-shifted differential chaos shift keying with code index modulation for high data rate transmission," *IEEE Trans. Commun.*, vol. 65, no. 10, pp. 4285–4294, Oct. 2017.
[22] W. Xu, Y. Tan, F. C. M. Lau, and G. Kolumbán, "Design and optimization of differential chaos shift keying scheme with code index modulation," *IEEE Trans. Commun.*, vol. 66, no. 5, pp. 1970–1980, May 2018.
[23] M. Herceg, G. Kaddoum, D. Vranješ, and E. Soujeri, "Permutation index DCSK modulation technique for secure multiuser high-data-rate communication systems," *IEEE Trans. Veh. Technol.*, vol. 67, no. 4, pp. 2997–3011, Apr. 2018.
[24] M. Herceg, D. Vranješ, G. Kaddoum, and E. Soujeri, "Commutation code index DCSK modulation technique for high-data-rate communication systems," *IEEE Trans. Circuits Syst., II, Exp. Briefs*, vol. 65, no. 12, pp. 1954–1958, Dec. 2018.
[25] B. Van Nguyen, M. T. Nguyen, H. Jung, and K. Kim, "Designing antijamming receivers for NR-DCSK systems utilizing ICA, WPD, and VMD methods," *IEEE Trans. Circuits Syst., II, Exp. Briefs*, to be published. doi: 10.1109/TCSII.2019.2891254.
[26] K. Raju, T. Ristaniemi, J. Karhunen, and E. Oja, "Jammer suppression in DS-CDMA arrays using independent component analysis," *IEEE Trans. Wireless Commun.*, vol. 5, no. 1, pp. 77–82, Jan. 2006.
[27] G. Kaddoum, N. Tadayon, and E. Soujeri, "Performance of DCSK system with blanking circuit for power-line communications," in *Proc. IEEE ISCAS*, Montreal, QC, Canada, May 2016, pp. 1118–1121.
[28] H. Yang and G.-P. Jiang, "High-efficiency differential-chaos-shift-keying scheme for chaos-based noncoherent communication," *IEEE Trans. Circuits Syst. II, Exp. Briefs*, vol. 59, no. 5, pp. 312–316, May 2012.
[29] S. V. Zhidkov, "Analysis and comparison of several simple impulsive noise mitigation schemes for OFDM receivers," *IEEE Trans. Commun.*, vol. 56, no. 1, pp. 5–9, Jan. 2008.
[30] F. H. Juwono, Q. Guo, D. Huang, Y. Chen, L. Xu, and K. P. Wong, "On the performance of blanking nonlinearity in real-valued OFDM-based PLC," *IEEE Trans. Smart Grid*, vol. 9, no. 1, pp. 449–457, Jan. 2018.
[31] S. Sedaghatnejad and M. Farhang, "Detectability of chaotic direct-sequence spread-spectrum signals," *IEEE Wireless Commun. Lett.*, vol. 4, no. 6, pp. 589–592, Dec. 2015.
[32] I. S. Gradshteyn and I. M. Ryzhik, *Table of Integrals, Series, and Products*, 7th ed. New York, NY, USA: Academic, 2007.

DUC-PHUC VUONG received the B.S. and M.S. degrees in marine electrical engineering and automation from Vietnam Maritime University (VMU), in 2004 and 2007, respectively, and the Ph.D. degree in electric and control engineering from Mokpo National Maritime University, South Korea, in 2014. He is currently a Lecturer with the Department of Electric and Electronics Engineering, VMU. His research interests include the control of industrial machines and robots, wireless communications and signal processing, and recycle energy.

DANG-KHANH LE received the B.S. degree from the Marine Engineering Department, Vietnam Maritime University (VMU), Haiphong, Vietnam, in 2006, and the M.S. and Ph.D. degrees from the Department of Marine Engineering, Mokpo National Maritime University (MMU), South Korea, in 2012 and 2016, respectively. He was a Postdoctoral Researcher with MMU, in 2016. He is currently a Lecturer with the VMU College, VMU. His research interests include instrumentation and automation control, UVA modeling and simulation, ultrasonic technologies and applications, iterative learning control, intelligent transportation systems, and wireless communications and signal processing.

KHAC-KHIEM NGUYEN received the B.S. degree in marine electrical engineering and automation from Vietnam Maritime University (VMU), the M.A. degree in system control from The University of New South Wales, Australia, in 1998, and the Ph.D. degree, in 2007. He is currently a Lecturer with the Department of Electric and Electronics Engineering, VMU. His research interests include the control of industrial machines and robots, recycle energy, ship power plants, and wireless communications and signal processing.

BINH VAN NGUYEN received the B.S. degree in electrical and electronics from the Ho Chi Minh City University of Technology, Ho Chi Minh City, Vietnam, in 2010, and the M.S. and Ph.D. degrees in wireless communications from the Gwangju Institute of Science and Technology, Gwangju, South Korea, in 2012 and 2016, respectively, where he is currently a Research Fellow. His research interests include cooperative communications, physical-layer security, chaotic and anti-jamming communications, and biomedical signal processing and application design.